Cardiovasc Intervent Radiol (2019) 42:1016–1023
https://doi.org/10.1007/s00270-019-02215-8

LABORATORY INVESTIGATION

Robotically Assisted Sonic Therapy (RAST) for Noninvasive Hepatic Ablation in a Porcine Model: Mitigation of Body Wall Damage with a Modified Pulse Sequence

Katherine C. Longo[1] · Emily A. Knott[1] · Rao F. Watson[2] · John F. Swietlik[1] · Eli Vlaisavljevich[6] · Amanda R. Smolock[7] · Zhen Xu[8] · Clifford S. Cho[9] · Lu Mao[4] · Fred T. Lee Jr.[1,3,5] · Timothy J. Ziemlewicz[1]

Received: 11 January 2019 / Accepted: 31 March 2019 / Published online: 30 April 2019

Abstract

Purpose Robotically assisted sonic therapy (RAST) is a nonthermal, noninvasive ablation method based on histotripsy. Prior animal studies have demonstrated the ability to create hepatic ablation zones at the focal point of an ultrasound therapy transducer; however, these treatments resulted in thermal damage to the body wall within the path of ultrasound energy delivery. The purpose of this study was to evaluate the efficacy and safety of a pulse sequence intended to mitigate prefocal body wall injury.

Materials and Methods Healthy swine ($n = 6$) underwent hepatic RAST (VortxRx software version 1.0.1.3, HistoSonics, Ann Arbor MI) in the right hepatic lobe. A 3.0 cm spherical ablation zone was prescribed for each. Following treatment, animals underwent MRI which was utilized for ablation zone measurement, evaluation of prefocal injury, and assessment of complications. Each animal was euthanized, underwent necropsy, and the tissue was processed for histopathologic analysis of the ablation zone and any other sites concerning for injury.

Results No prefocal injury was identified by MRI or necropsy in the body wall or tissues overlying the liver. Ablation zones demonstrated uniform cell destruction, were nearly spherical (sphericity index = 0.988), and corresponded closely to the prescribed size (3.0 × 3.1 × 3.4 cm, $p = 0.70$, 0.36, and 0.01, respectively). Ablation zones were associated with portal vein ($n = 3$, one occlusive) and hepatic vein thrombosis ($n = 4$, one occlusive); however, bile ducts remained patent within ablation zones ($n = 2$).

Conclusions Hepatic RAST performed with a modified ultrasound pulse sequence in a porcine model can mitigate prefocal body wall injuries while maintaining treatment efficacy. Further study of hepatic RAST appears warranted, particularly in tumor models.

Keywords Histotripsy · Ablation · Ultrasound · RAST · Interventional oncology

✉ Katherine C. Longo
klongo@uwhealth.org

1 Department of Radiology, University of Wisconsin Hospital and Clinics, 600 Highland Ave, Madison, WI 53705, USA

2 Department of Pathology, University of Wisconsin, Madison, USA

3 Department of Biomedical Engineering, University of Wisconsin, Madison, USA

4 Department of Biostatistics and Medical Informatics, University of Wisconsin, Madison, USA

5 Department of Urology, University of Wisconsin, Madison, USA

6 Department of Biomedical Engineering and Mechanics, Virginia Polytechnic and State University, Blacksburg, USA

7 Division of Interventional Radiology, Department of Radiology, University of Pennsylvania, Philadelphia, USA

8 Department of Biomedical Engineering, University of Michigan, Ann Arbor, USA

9 Department of Surgery, University of Michigan, Ann Arbor, USA

Introduction

Liver tumors remain a substantial worldwide health problem despite recent improvements in surgery, radiation, ablation, and chemotherapy. Currently, thermal ablation is first-line therapy for small hepatocellular carcinoma and second line for patients with inoperable hepatic colorectal

metastases [1, 2]. Unfortunately, there are significant limitations to thermal ablation techniques including complications from applicator placement, safety limitations for treating tumors in central locations and near bile ducts, a thermal "penumbra" in which sublethal heating may paradoxically increase the risk of local recurrence and also promote systemic tumor growth, and substantial procedural complexity with a dependence on operator expertise leading to highly variable outcomes [3–6].

Histotripsy is a noninvasive and nonthermal ablation modality which destroys tissue at the subcellular level by producing cavitation in the targeted tissue [7]. The technique is based on high-intensity, low-duty-cycle pulses of focused ultrasound that converge at a focal point. There is no increase above body temperature within the ablation zone since the cellular destruction is mechanically based and not heat-based. Importantly, histotripsy is a binary process in which cavitation only occurs when a threshold has been reached, thus potentially avoiding damage to nontarget structures [8–11]. When combined with a robotic arm and software control to deliver a specific ablation size, shape, and volume, the procedure is termed robotically assisted sonic therapy (RAST). To date, hepatic RAST has only been used to create ablation zones in large animal models in limited proof of concept and safety studies [12–14]. The results of these investigations which were recently published have demonstrated the ability of RAST to create spherical ablation zones up to 3 cm in size with complete central ablation. In contrast to currently available thermal ablation modalities, bile ducts within and adjacent to the ablation zone were spared. This is likely due to the increased tensile strength of the bile ducts which make them more resistant to cavitation. One-month follow-up examinations demonstrated involution of the ablation zone, and there was no significant surrounding inflammation evident acutely or at follow-up [14].

The main limitation identified in the prior proof of concept hepatic RAST study was variably occurring, limited thermal damage to the body wall overlying the hepatic ablation [14]. Although histotripsy destroys tissue via mechanical effects at the focal point, energy deposition along the ultrasound delivery path can lead to heat creation. This damage was generally seen in cases where the ultrasound window was substantially limited due to overlying rib coverage and/or an air-filled stomach, necessitating an increase in amplitude to create a cavitation bubble cloud. This increased amplitude combined with a pulse sequence which was not specifically designed to limit thermal energy deposition was the likely etiology for the body wall thermal injuries. Following the proof of concept RAST study, a software upgrade with an improved thermal profile was made available. Thus, the purpose of this study was to evaluate whether hepatic RAST performed with this improved thermal profile can produce uniform cell destruction within the targeted ablation zone while avoiding prefocal thermal body wall injury.

Methods

Experimental Design

Six healthy female swine (mean weight 55 kg, Arlington, WI) underwent hepatic RAST followed by MRI without and with intravenous contrast. Animals were then immediately killed for necropsy and tissue harvesting for histopathology.

Animal Handling and Anesthesia

All animal care and procedures were approved by the Institutional Animal Care and Use Committee. There were no techniques used to control for respiratory motion during the ablation. Prior to treatment, the animals were premedicated with 325 mg aspirin orally the evening prior to the procedure and 40 mg enoxaparin subcutaneously immediately before RAST. Animals were positioned dorsal recumbent on a surgical table throughout the procedure.

RAST

All RAST ablations were performed with a prototype system using a custom 700 kHz multi-element therapy transducer powered by a therapeutic ultrasound signal generator and amplifier (VortxRx, HistoSonics, Inc., Ann Arbor, MI). The system also utilized a 3 MHz curvilinear array ultrasound transducer (Model C5-2, Analogic Corp., Peabody, MA) which is co-axially aligned through a central aperture in the therapy transducer, allowing real-time ultrasound guidance for targeting and monitoring. The therapy and imaging transducers are attached to a robotic arm and driven by micro-positioning motors capable of movement in the x, y, and z planes. The transducer position is controlled by a proprietary software package through which the operator can prescribe virtually any size, shape, and volume of ablation [14].

Treatments were delivered using the VortxRx software version 1.0.1.3 (HistoSonics, Inc., Ann Arbor, MI). This version reduced the time-average intensity of energy delivery by greater than 60% compared to the prior version that produced body wall injuries in some subjects [14]. A 3 cm spherical treatment volume was prescribed in the right lobe of the liver in the planning phase of the procedure. Ultrasound energy was delivered to generate a bubble cloud within the planned ablation zone, controlled by the proprietary software, with the treating physician

monitoring the bubble cloud in real time using the co-axially aligned diagnostic ultrasound transducer. This real-time bubble cloud tracking enabled the treating physician to verify treatment delivery to the entire planned ablation zone.

Magnetic Resonance Imaging

Following completion of the ablation, the animals were imaged on a 3T MRI (GE Signa Pet MR or GE Healthcare Discovery MR 750/750 W, Waukesha, WI). Prior to contrast administration, coronal SSFSE, axial STIR, in-/out-of-phase T1, axial T2, and axial GRE T1 sequences of the abdomen were obtained. Following the administration of 0.06 mmol/kg body weight of gadoxetate disodium (Eovist, Bayer Healthcare, Whippany, NJ) injected at a rate of 2 mL/s, axial GRE T1 sequences of the abdomen were obtained in the late arterial, portal venous, 5-min delay, and 20-min delay (hepatobiliary) phases. Coronal T1 GRE and LAVA FLEX axial sequences were also obtained approximately 20 min post-contrast injection.

Imaging Analysis

MR images were analyzed in consensus on an institutional PACS station (McKesson, San Francisco, CA) by radiologists with 2–12 years of image interpretation experience. All measurements were made in the portal venous phase. Orthogonal AP and transverse measurements were made in the axial plane, and one craniocaudal measurement was made in the coronal plane. These measurements were used to calculate sphericity index as described below. Ablation zone volumes were directly measured using a volume rendering software package (Vitrea, Vital Images, Minnetonka, MN).

Pathology

After euthanasia, necropsy was performed and adjacent structures were inspected for gross signs of injury. The livers were harvested, and microscopic pathology was analyzed by a dedicated liver pathologist. Measurements were obtained from eight separate sites around the periphery of each ablation zone to determine a mean thickness of the zone of partial tissue disruption.

Statistical Analysis

Statistical analysis was performed using R version 3.3.2 (R Core Team, 2014, R Foundation for Statistical Computing, Vienna, Austria; available at: http://www.R-project.org/). Measurements of volume and sizes (trans, AP, CC) of the ablation zone were summarized by mean ± standard deviation. The means were compared with the prescribed values using two-sided t tests. The sphericity index for each subject was calculated using the formula:

$$\Psi = p^{1/3}(6V)^{2/3}/SA$$

where V represents volume and SA surface area [15]. The volume and the surface area were calculated assuming that the ablation zone is a spheroid with equatorial radius approximated by the average of the more similar measurements and polar radius approximated by the most extreme measurement [15]. The mean (± standard deviation) of the resulting sphericity indices was compared to 1 using a one-sided t test.

Results

Off-Target Injury

There was no MR evidence of edema, hemorrhage, or enhancement within the body wall to suggest body wall injury in any of the subjects, and there was no evidence of body wall injury at necropsy (Fig. 1). In one subject, the ablation zone abutted the cranial aspect of the gallbladder. A trace amount of inherently T1 hyperintense fluid was seen layering dependently within the gallbladder lumen consistent with blood products. The gallbladder wall was intact and there was no evidence of gallbladder rupture (Fig. 2).

At necropsy, the peritoneum, body wall, and adjacent organs demonstrated no evidence of bleeding, contusion or thermal injuries with the exception of one case in which the ablation zone abutted the diaphragm. In that case, the ablation zone appeared to extend into the diaphragm and lower lung, therefore both organs were excised and submitted for histopathologic examination.

Ablation Zone

All ablations were created within the right lobe of the liver. The overall mean depth measured from the skin surface to the center of the ablation zone was 8.2 cm (6.7–10.0). Mean ablation zone size was 3.0 (trans) × 3.1 (AP) × 3.4 cm (CC) with a mean sphericity index of 0.988 (Table 1). The ablation zone appearance was similar in appearance to previous descriptions: inherently T1 hyperintense, minimally hyperintense on T2WI, no appreciable enhancement or surrounding hyperemia after contrast administration, and without diffusion restriction [14]. On gross pathology, the hepatic ablation zones were well demarcated with a red central region surrounded by a thin

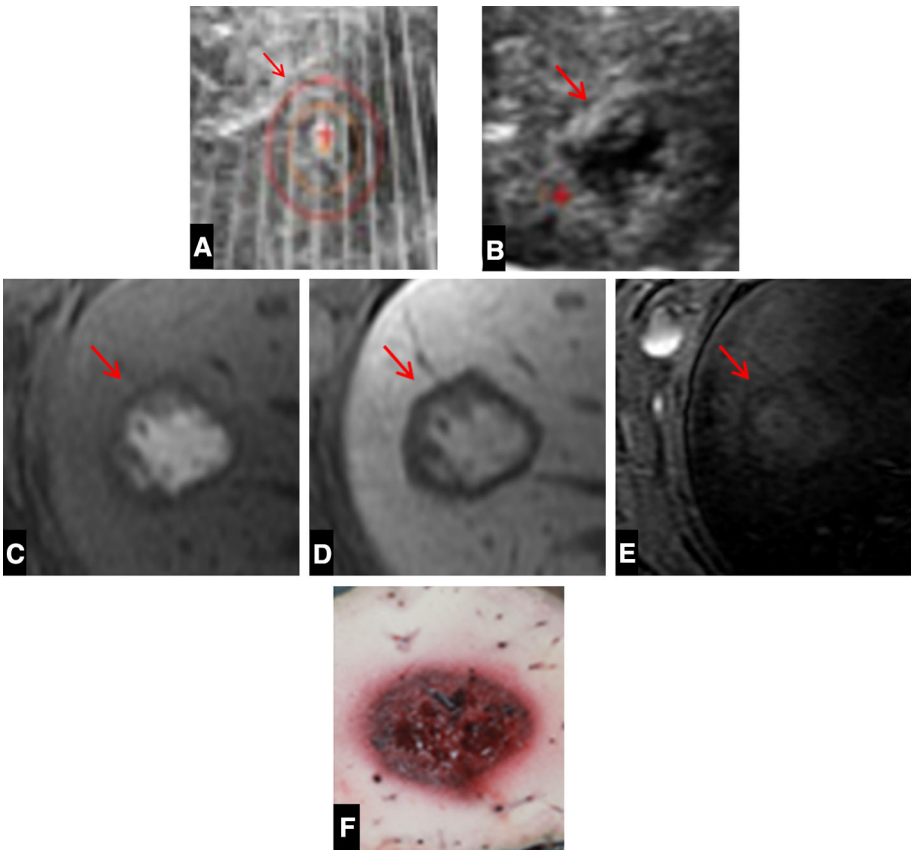

Fig. 1 **A** Intra-procedural ultrasound image demonstrating the bubble cloud (arrow) within the right hepatic lobe. **B** Corresponding immediate post-procedure image shows the hypoechoic ablation zone (arrow). **C** Axial T1 pre-contrast images demonstrate a well-demarcated ablation zone (arrow) containing high-signal-intensity blood products. **D** Axial T1 post-contrast portal venous phase MRI image with no enhancement. **E** Axial STIR image demonstrates no evidence of body wall edema or injury. **F** Corresponding gross pathologic specimen of the liver with a well-demarcated ablation zone without damage to the surrounding liver. The thin area of light red tissue surrounding the ablation zone corresponds to the transition zone

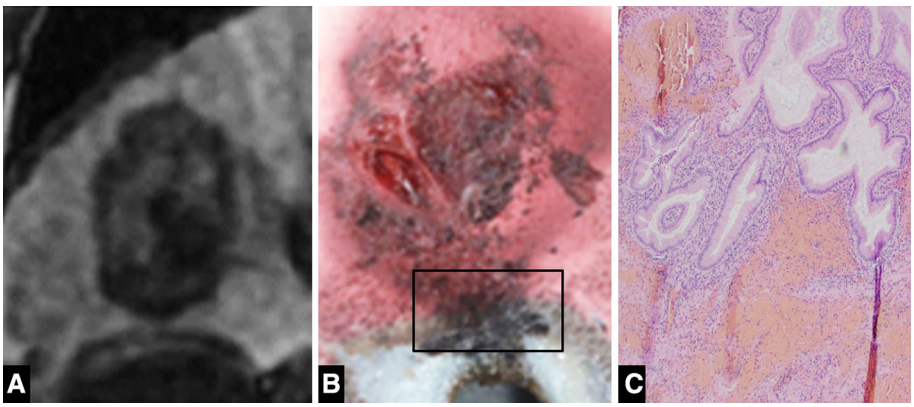

Fig. 2 **A** Coronal 20-min delay MRI image demonstrating the close proximity of the ablation zone to the cranial aspect of the gallbladder. **B** Gross pathologic specimen demonstrates extension of the ablation zone to involve the gallbladder fossa. **C** Histology (× 100) demonstrates hemorrhage within the gallbladder wall with intact mucosa

zone of transition to normal appearing liver (Fig. 1). The mean transition diameter was 3.9 mm (SD 2.5 mm).

Vessels and Bile Ducts

Three animals had portal vein thrombus and four animals had hepatic vein thrombus following RAST (Fig. 3). In all cases, the ablation zones overlapped the vessels containing thrombus with propagation of thrombus outside of the ablation zone. Two of the three portal vein thromboses were in the main portal vein, and one was in a peripheral portal vein distal to the ablation zone. The two cases of main portal vein thrombus were nonocclusive. The one case of thrombus in a peripheral portal vein branch was occlusive. All four cases of hepatic vein thrombus were central to the ablation zone. One of the four cases was occlusive while the remaining three cases were nonocclusive (Table 1). Four ablations were associated with a zone of hypoperfusion peripheral to the ablation zone due to portal and/or hepatic vein thrombus.

On hepatobiliary phase imaging of two subjects, a patent bile duct containing Eovist was seen traversing the periphery of the ablation zone (Fig. 4).

Table 1 Description of RAST ablations

Subject number	Trans (cm)	AP (cm)	CC (cm)	Volume	Sphericity index	Mean transition zone (SD) (mm)	Main portal vein thrombus	Peripheral portal vein thrombus	Main hepatic vein thrombus	Peripheral hepatic vein thrombus	Body wall injury
3135	2.9	3.0	3.4	20	0.997	2.8 (1.6)	N	Y occlusive distally	N	N	N
3137	3.2	3.2	3.3	17.2	1.000	5.3 (3.4)	Y nonocclusive	N	Y nonocclusive	N	N
3138	3.1	3.2	3.7	19.3	0.996	3.8 (2.8)	N	N	N	N	N
3139	2.7	2.9	3.6	13.3	0.989	0.5 (0.2)	N	N	Y nonocclusive	N	N
3148	3.2	3.0	3.3	17	0.961	4.3 (2.9)	N	N	Y occlusive	N	N
3149	3.1	3.0	3.1	16.7	0.984	2.5 (1.4)	Y nonocclusive	N	Y nonocclusive	N	N

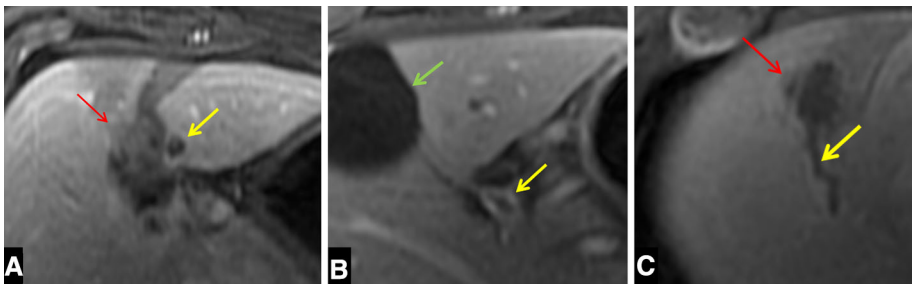

Fig. 3 **A** Axial portal venous phase MRI demonstrates an occlusive portal vein thrombus (yellow arrow) distal to the ablation zone (red arrow). **B** Axial portal venous phase imaging of a different subject demonstrates nonocclusive proximal portal vein thrombus (yellow arrow) The gallbladder is also in view (green arrow). **C** Axial portal venous phase image of a third subject demonstrates nonocclusive hepatic vein thrombus (yellow arrow) adjacent to the ablation zone (red arrow)

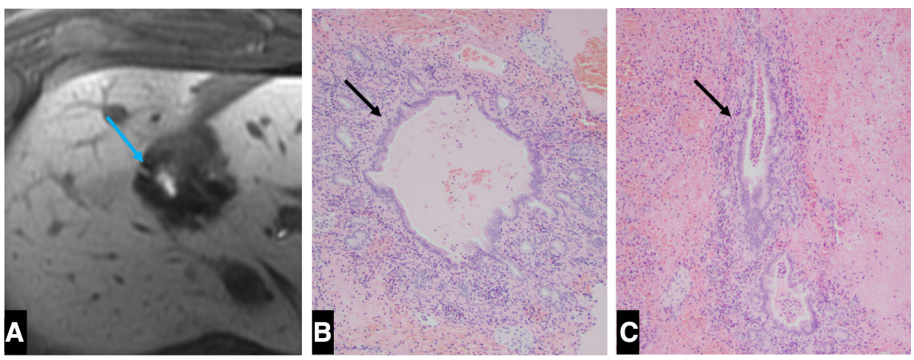

Fig. 4 **A** Axial post-contrast 20 min delayed image demonstrates a patent bile duct containing Eovist within the ablation zone (blue arrow). **B**, **C** Histology (× 100) demonstrating the intact bile duct at the periphery of the ablation zone (green arrows)

Pathology

All ablation zones demonstrated a well-circumscribed zone of complete tissue destruction. Within the central ablation zone, there was a small amount of residual fibrinous material, blood, and scattered nuclear fragments. There were a few small clusters of hepatocytes present, but they are not deemed as viable as they were entirely detached from the normal sinusoidal framework and portal vasculature. There was a thin transition zone of partial ablation with a mean diameter of 3.9 mm (SD 2.5 mm), ranging from 0.1 to 0.9 mm (Fig. 5). The uninvolved hepatic tissues adjacent to the ablation zone (within ~ 1 cm) showed patchy sinusoidal dilation with congestion and edema. There was no unexpected hemorrhage within the liver. Within one of the ablation zones, viably large bile ducts were present at the periphery (Fig. 4).

In the animal where the ablation zone extended into the diaphragm, there were findings suggestive of ablation effect within the adjacent diaphragm and lung parenchyma, though the collagenous architecture of these structures was maintained. In the animal where the ablation zone extended to involve the gallbladder fossa, the gallbladder bed showed hemorrhage that extended into the gallbladder

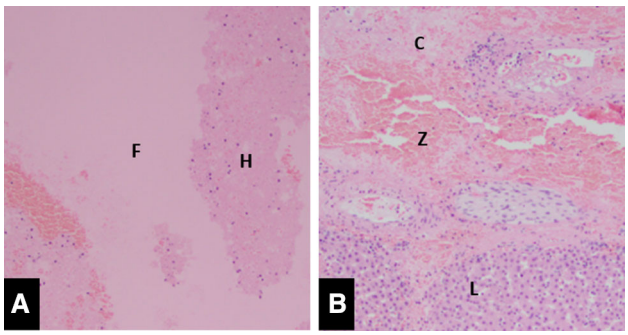

Fig. 5 **A** Microscopic image (× 100) of the center of the ablation zone demonstrates a few small clusters of detached non-viable hepatocytes (H) and fibrinous debris (F) present. **B** Microscopic image (× 100) of the periphery of the ablation shows viable liver (L) liver with complete ablation effect (**C**) and a thin zone of transition (Z)

muscular wall; however, the mucosal epithelium was not involved and showed no evidence of necrosis (Fig. 2).

Discussion

RAST is a noninvasive and nonthermal ablation modality based on histotripsy that is currently being evaluated for use in the treatment of human liver tumors. The results of this study demonstrated that RAST performed using a modified pulse sequence produced effective ablation zones in the porcine liver without causing thermal body wall injuries, an important advance compared to an earlier proof of concept study [14]. As before, the ablation zones corresponded closely to the prescribed values in size and shape with a slightly larger CC measurement due to respiratory motion which was not controlled for (Table 2). Mean ablation zone size in the current study was 3.0 (trans) × 3.1 (AP) × 3.4 cm (CC) with a mean sphericity index of 0.988 (Table 1). This is similar to the previous proof of concept study which showed a mean ablation size of 3.2 (trans) × 3.0 (AP) and 3.8 (CC) with a mean sphericity index of 0.986. There was no change in efficacy with the modified pulse sequence demonstrating thorough destruction of tissue within the ablation zone.

Table 2 Actual ablation zone sizes versus prescribed (n = 6)

	Prescribed	Actual	p
Volume (mL)	14	17.25 ± 2.35	0.020
Anteroposterior (cm)	3.0	3.03 ± 0.20	0.696
Transverse (cm)	3.0	3.05 ± 0.12	0.363
Craniocaudal (cm)	3.0	3.40 ± 0.22	0.007
Sphericity index	1	0.988 ± 0.014	0.043

Histotripsy is applied in a similar fashion to thermal high-intensity focused ultrasound (thermal HIFU) in that both methods use externally applied focused ultrasound to destroy tissue, but unlike thermal HIFU, the mechanism of ablation with histotripsy is mechanical cavitation, not heat. Histotripsy uses high-intensity ultrasound pulses at low duty cycles (< 1%) to create cavitation and mechanical tissue destruction at the subcellular level without significant heating [8–11]. In contrast, thermal HIFU heats tissue through the application of continuous or near-continuous lower energy ultrasound. As a result, thermal HIFU is susceptible to all of the known limitations of thermal ablation modalities including the heat sink effect near large blood vessels, a thermal penumbra of sublethal heating surrounding the ablation zone which may have negative local and systemic effects, and damage to thermally sensitive structures such as bowel and bile ducts [16–19].

One interesting aspect of histotripsy is the binary nature of tissue destruction which only occurs once a cavitation threshold has been reached. High tensile strength structures such as bile ducts and blood vessels are more resistant to cavitation-induced tissue damage due to higher mechanical strength [20]. This tissue selectivity is potentially important when translating to clinical human use due to the possibility of safer treatments for central hepatic tumors, a current weakness of thermal ablation devices [3–6].

RAST has only recently been applied to human-scale porcine livers, the most widely used preclinical model for evaluating ablation devices [12–14, 21, 22]. There is a large body of histotripsy literature in small animal models, including treatment of implanted tumors in which histotripsy was able to completely destroy targeted tissue; the homogenate was rapidly resorbed, and animals demonstrated prolonged survival [9, 23–25]. However, the use of a small animal system and small animal implanted tumor models raises questions as to the applicability for human tumors in terms of both scale and biologic response. More recent studies in a porcine model were performed using hardware and software that is being evaluated for potential human clinical use. The results of these studies have demonstrated the safety of applying histotripsy in perivascular territories, the ability to create larger spherical ablation zones appropriate for human use, and the effect of histotripsy on major bile ducts [12–14]. This study also demonstrated resolution of associated vascular thrombus and significant involution of the ablation zone over 30 days. Given the body wall injuries previously noted on fluid sensitive MRI sequences and a desire to minimize side effects of this noninvasive treatment, a software upgrade was performed which modified the pulse sequence, intending to minimize thermal dose delivery to the abdominal wall. In the current study, the pulse sequence was evaluated and noted to avoid the thermal

damage along the beam path seen previously on MRI images while still producing effective ablation zones.

An interesting finding in this study was the thin transition zone between ablated and normal parenchyma of 3.9 mm despite not controlling for respiratory motion. This transition zone is similar to the tightest of those identified by Cornelis, et al. [26] when studying currently available ablation modalities, with a 3.2 mm and 4.5 mm average transition zone identified for microwave and cryoablation, respectively. This similarity occurs despite the energy being delivered from an external source rather than an internal needle-based source which is "locked" in place during treatment. As the ablation zones are elongated in the craniocaudal dimension, it could be postulated that this accounted for the larger transition zones (up to 0.9 mm), while the smaller (as low as 0.1 mm) were in the axial plane. The study was not designed to control for this and this is a potential area for future evaluation, particularly as the procedure may benefit from being performed with compensatory measures, such as electronic beam-steering or jet ventilation [27]. An additional strategy to overcome respiratory motion would be respiratory gating and intermittent application of RAST. However, this is associated with a substantial time penalty.

This study has several limitations. All experiments were performed in a normal porcine model due to the lack of available pig tumor models. Pigs have major anatomical differences in hepatic anatomy compared to humans with a thin, flat, multilobar, cranially positioned liver which is often underlying a large gas-filled stomach and closely spaced ribs that can limit the acoustic window [28]. Based on our prior experience with thermal ablation and histotripsy in pigs, a 3 cm ablation is the largest ablation that could consistently fit into a porcine liver. Even with this limitation in ablation zone size, in one subject the ablation extended into the diaphragm and lung base, and in another subject the ablation zone extended into the gallbladder, likely a result of both the flat pig liver and respiratory motion which is most pronounced in the craniocaudal direction. Human livers are larger and more caudally positioned with a better ultrasound window, aided by a smaller (presumably less gas-filled) stomach due to better control of ingested materials. Other limitations to this study included lack of chronic follow-up to evaluate the evolution of the ablation zone and vascular thrombus. However, a previous study by Smolock et al. [14] included a 1-month survival arm, and thus, reconfirmation of the chronic findings of that study was not felt to be necessary in this study that focused on reducing the potential for prefocal thermal injury.

In summary, hepatic RAST performed using software optimized to produce less prefocal heating created well circumscribed, near-spherical ablation zones with uniform central necrosis that closely adhered to the prescribed size and shape without the undesirable side effect of body wall injury. Continued study of RAST, particularly in tumor models, appears warranted.

All applicable international, national, and/or institutional guidelines for the care and use of animals were followed. All procedures performed in studies involving animals were in accordance with the ethical standards of the institution or practice at which the studies were conducted.

Acknowledgements The authors would like to acknowledge the HistoSonics R&D team, Jim Bertolina, Jon Cannata, Alex Duryea, Ryan Miller, and Zeljko Mladenovic for developing the pulse sequence evaluated in this study and for technical support during the study.

Funding This study was funded by HistoSonics, Inc.

Compliance with Ethical Standards

Conflict of interest The authors of this manuscript declare relationships with the following companies: Fred T. Lee Jr., MD—Ethicon, Inc.: Consultant, HistoSonics, Inc.: Board Member, Advisor, Stockholder. Amanda Smolock MD, PhD—HistoSonics, Inc.: Advisor, Stockholder. Eli Vlaisavljevich, PhD—HistoSonics, Inc.: Advisor, Stockholder. Zhen Xu, PhD—HistoSonics, Inc.: Founder, Advisor, Stockholder. Timothy Ziemlewicz, MD—Ethicon, Inc.: Consultant, HistoSonics, Inc.: Advisor, Stockholder.

Ethical Approval All applicable international, national, and/or institutional guidelines for the care and use of animals were followed. All procedures performed in studies involving animals were in accordance with the ethical standards of the institution or practice at which the studies were conducted. Approval was obtained from the Institutional animal use and care committee.

References

1. Llovet JM, Fuster J, Bruix J. The Barcelona approach: diagnosis, staging, and treatment of hepatocellular carcinoma. Liver Transpl. 2004;10:S115–20. https://doi.org/10.1002/lt.20034.
2. Ziemlewicz TJ, Wells SA, Lubner MG, et al. Hepatic tumor ablation. Surg Clin North Am. 2016;96:315–39. https://doi.org/10.1016/j.suc.2015.12.006.
3. Lahat E, Eshkenazy R, Zendel A, et al. Complications after percutaneous ablation of liver tumors: a systematic review. Hepatobiliary Surg Nutr. 2014;3:317–23. https://doi.org/10.3978/j.issn.2304-3881.2014.09.07.
4. Livraghi T, Meloni F, Solbiati L, et al. Complications of microwave ablation for liver tumors: results of a multicenter study. Cardiovasc Intervent Radiol. 2012;35:868–74. https://doi.org/10.1007/s00270-011-0241-8.
5. Velez E, Goldberg SN, Kumar G, et al. Hepatic thermal ablation: effect of device and heating parameters on local tissue reactions and distant tumor growth. Radiology. 2016;281:782–92. https://doi.org/10.1148/radiol.2016152241.
6. Poon RT, Ng KK, Lam CM, et al. Learning curve for radiofrequency ablation of liver tumors—prospective analysis of initial 100 patients in a tertiary institution. Ann Surg. 2004;239:441–9. https://doi.org/10.1097/01.sla.0000118565.21298.0a.

7. Hall TL, Hempel CR, Wojno K, et al. Histotripsy of the prostate: dose effects in a chronic canine model. Urology. 2009;74:932–7. https://doi.org/10.1016/j.urology.2009.03.049.
8. Parsons JE, Cain CA, Abrams GD, et al. Pulsed cavitational ultrasound therapy for controlled tissue homogenization. Ultrasound Med Biol. 2006;32:115–29. https://doi.org/10.1016/j.ultrasmedbio.2005.09.005.
9. Roberts WW, Hall TL, Ives K, et al. Pulsed cavitational ultrasound: a noninvasive technology for controlled tissue ablation (histotripsy) in the rabbit kidney. J Urol. 2006;175:734–8. https://doi.org/10.1016/s0022-5347(05)00141-2.
10. Xu Z, Ludomirsky A, Eun LY, et al. Controlled ultrasound tissue erosion. IEEE Trans Ultrason Ferroelectr Freq Control. 2004;51:726–36.
11. Vlaisavljevich E, Maxwell A, Mancia L, et al. Visualizing the histotripsy process: bubble cloud-cancer cell interactions in a tissue-mimicking environment. Ultrasound Med Biol. 2016;42:2466–77. https://doi.org/10.1016/j.ultrasmedbio.2016.05.018.
12. Vlaisavljevich E, Owens G, Lundt J, et al. Non-invasive liver ablation using histotripsy: preclinical safety study in an in vivo porcine model. Ultrasound Med Biol. 2017;43:1237–51. https://doi.org/10.1016/j.ultrasmedbio.2017.01.016.
13. Vlaisavljevich E, Kim Y, Allen S, et al. Image-guided non-invasive ultrasound liver ablation using histotripsy: feasibility study in an in vivo porcine model. Ultrasound Med Biol. 2013;39:1398–409. https://doi.org/10.1016/j.ultrasmedbio.2013.02.005.
14. Smolock AR, Cristescu MM, Vlaisavljevich E, et al. Robotically assisted sonic therapy as a noninvasive nonthermal ablation modality: proof of concept in a porcine liver model. Radiology. 2018. https://doi.org/10.1148/radiol.2018171544.
15. Wadell H. Volume, shape, and roundness of quartz particles. J Geol. 1935;43:250–80. https://doi.org/10.1086/624298.
16. Li JJ, Gu MF, Luo GY, et al. Complications of high intensity focused ultrasound for patients with hepatocellular carcinoma. Technol Cancer Res Treat. 2009;8:217–24. https://doi.org/10.1177/153303460900800306.
17. ter Haar G. High intensity ultrasound. Semin Laparosc Surg. 2001;8:77–89. https://doi.org/10.1177/155335060100800109.
18. Jung SE, Cho SH, Jang JH, et al. High-intensity focused ultrasound ablation in hepatic and pancreatic cancer: complications. Abdom Imaging. 2011;36:185–95. https://doi.org/10.1007/s00261-010-9628-2.
19. Khokhlova TD, Wang YN, Simon JC, et al. Ultrasound-guided tissue fractionation by high intensity focused ultrasound in an in vivo porcine liver model. Proc Natl Acad Sci USA. 2014;111:8161–6. https://doi.org/10.1073/pnas.1318355111.
20. Vlaisavljevich E, Kim Y, Owens G, et al. Effects of tissue mechanical properties on susceptibility to histotripsy-induced tissue damage. Phys Med Biol. 2014;59:253–70. https://doi.org/10.1088/0031-9155/59/2/253.
21. Harari CM, Magagna M, Bedoya M, et al. Microwave ablation: comparison of simultaneous and sequential activation of multiple antennas in liver model systems. Radiology. 2016;278:95–103. https://doi.org/10.1148/radiol.2015142151.
22. Yu NC, Raman SS, Kim YJ, et al. Microwave liver ablation: influence of hepatic vein size on heat-sink effect in a porcine model. J Vasc Interv Radiol. 2008;19:1087–92. https://doi.org/10.1016/j.jvir.2008.03.023.
23. Styn NR, Wheat JC, Hall TL, et al. Histotripsy of VX-2 tumor implanted in a renal rabbit model. J Endourol. 2010;24:1145–50. https://doi.org/10.1089/end.2010.0123.
24. Lake AM, Hall TL, Kieran K, et al. Histotripsy: minimally invasive technology for prostatic tissue ablation in an in vivo canine model. Urology. 2008;72:682–6. https://doi.org/10.1016/j.urology.2008.01.037.
25. Hempel CR, Hall TL, Cain CA, et al. Histotripsy fractionation of prostate tissue: local effects and systemic response in a canine model. J Urol. 2011;185:1484–9. https://doi.org/10.1016/j.juro.2010.11.044.
26. Cornelis FH, Durack JC, Kimm SY, et al. A comparative study of ablation boundary sharpness after percutaneous radiofrequency, cryo-, microwave, and irreversible electroporation ablation in normal swine liver and kidneys. Cardiovasc Intervent Radiol. 2017;40:1600–8. https://doi.org/10.1007/s00270-017-1692-3.
27. Denys A, Lachenal Y, Duran R, et al. Use of high-frequency jet ventilation for percutaneous tumor ablation. Cardiovasc Intervent Radiol. 2014;37:140–6. https://doi.org/10.1007/s00270-013-0620-4.
28. Nykonenko A, Vavra P, Zonca P. Anatomic peculiarities of pig and human liver. Exp Clin Transplant. 2017;15:21–6.